

A Bayesian algorithm for model selection applied to caustic-crossing binary-lens microlensing events

N. Kains¹ \star , P. Browne², K. Horne², M. Hundertmark², A. Cassan³

¹*European Southern Observatory, Karl-Schwarzschild Straße 2, 85748 Garching bei München, Germany*

²*SUPA, School of Physics and Astronomy, University of St. Andrews, North Haugh, St Andrews, KY16 9SS, United Kingdom*

³*Institut d’Astrophysique de Paris, UMR7095 CNRS-Université Pierre & Marie Curie, 98 bis boulevard Arago, 75014 Paris, France*

Accepted ... Received ... ; in original form ...

ABSTRACT

We present a full Bayesian algorithm designed to perform automated searches of the parameter space of caustic-crossing binary-lens microlensing events. This builds on previous work implementing priors derived from Galactic models and geometrical considerations. The geometrical structure of the priors divides the parameter space into well-defined boxes that we explore with multiple Monte Carlo Markov Chains. We outline our Bayesian framework and test our automated search scheme using two data sets: a synthetic lightcurve, and the observations of OGLE-2007-BLG-472 that we analysed in previous work. For the synthetic data, we recover the input parameters. For OGLE-2007-BLG-472 we find that while χ^2 is minimised for a planetary mass-ratio model with extremely long timescale, the introduction of priors and minimisation of BIC, rather than χ^2 , favours a more plausible lens model, a binary star with components of 0.78 and 0.11 M_{\odot} at a distance of 6.3 kpc, compared to our previous result of 1.50 and 0.12 M_{\odot} at a distance of 1 kpc.

Key words: gravitational lensing, extrasolar planets, modelling, bayesian methods

1 INTRODUCTION

Gravitational microlensing (Einstein 1936) is a well-established technique to detect extrasolar planets (e.g. Mao & Paczyński 1991, Beaulieu et al. 2006, Muraki et al. 2011), and is complementary to other methods, being able to probe low-mass cool planets that are inaccessible to them from the ground. This allows us to carry out statistical studies of planets of all masses located at a few AU from their host star (Cassan et al. 2012). Microlensing occurs when one or several compact objects are located between a source star and the observer, leading to a gravitational deflection of the light from the source star by the “lens” objects. As the source and lens move in and out of alignment, this deflection is observable in the form of a simple characteristic brightening and fading pattern when the lensing object is a single star (Paczynski 1986), but takes a much more complex form when the lens is made up of more than one object. When that happens, the lightcurve typically features “anomalies”, which can be modelled to determine the nature of the lensing system. One of the configurations that can lead to anomalies is when the lensing system contains one or more planets. In order to determine the properties of

these planets, the anomalies must be analysed through detailed modelling; this paper is concerned with cases where the lens consists of two components.

Analysing anomalous microlensing lightcurves can be a significant computational challenge for a number of reasons. The calculation of a full binary-lens lightcurve, including the effects of having an extended source, is an expensive process computationally, and the parameter space to be explored is complex, with several degeneracies (e.g. Kubas et al. 2005). This is the case even when second-order effects, such as that of parallax due to the Earth’s orbit or orbital motion in the lensing system, are ignored.

A significant number of the ~ 1500 microlensing events now being discovered by survey teams in a season exhibit anomalies due to stellar or planetary companions to the lens star. Many of these are caustic-crossing events in which the lightcurve exhibits rapid jumps, brightening when a new pair of images forms and fading when two images merge and disappear. Cassan (2008) introduced an advantageous parameterisation for caustic-crossing events by linking two parameters, t_{in} and t_{out} , to the caustic-crossing times and two parameters, s_{in} and s_{out} , to the ingress and egress points where the source-lens trajectory crosses the caustic curve. These parameters make it easier to locate all possible source-lens trajectories that fit the observed caustic-crossing features.

\star email:nkains@eso.org

Kains et al. (2009) used the Cassan (2008) parameters to analyse the observed lightcurve of the microlensing event OGLE-2007-BLG-472, which exhibits two strong caustic-crossing features separated by about 3 days. This short duration suggested that the anomaly could be due to the source crossing a small planetary caustic, motivating detailed modelling to rule out alternative binary star lens models. The lowest- χ^2 model has a planetary mass ratio, but an extremely long event timescale, $t_E \sim 2000$ days, much longer than the 2-200 day range typical of Galactic Bulge microlensing events. On this basis Kains et al. (2009) rejected the global χ^2 minimum by placing an ad-hoc 300 day cutoff on t_E , and suggested that a Bayesian approach including appropriate priors on all the parameters would more naturally shift the posterior probability to local χ^2 minima with less extreme parameters.

Cassan et al. (2010) derived analytic formulae for the prior $\pi(s_{\text{in}}, s_{\text{out}})$ corresponding to a uniform and isotropic distribution of lens-source trajectories, which are specified by an angle α and impact parameter u_0 . A suitable prior on t_E arises by using a model of microlensing in the Galaxy to determine distributions for the lens and source distances and their relative proper motion, or alternatively by using a parameterised model fitted to the observed distribution of t_E among all the events found in the microlensing survey. In either case a prior on t_E effectively penalises very long and very short events, lowering the posterior probability of the $t_E \sim 2000$ d global χ^2 minimum found for OGLE-2007-BLG-472 and favouring local minima with more typical event timescales. Priors on other parameters can also be derived from models of stellar population synthesis such as the Besançon model (Robin et al. 2003), which we use in this work.

In this paper we develop further the Bayesian analysis of caustic-crossing events, exploiting intrinsic features of the $\pi(s_{\text{in}}, s_{\text{out}})$ prior to specify and test a procedure suitable for automatic exploration of the full parameter space. We test the procedure using synthetic lightcurve data, and we re-analyse the OGLE-2007-BLG-472 data to compare the results of maximum likelihood analysis (χ^2 minimisation) with the full Bayesian analysis including appropriate priors.

2 BINARY-LENS MICROLENSING

In the context of microlensing, caustics are locations in the source plane, behind the lens, where the magnification is infinite. A point-mass lens produces a point caustic directly behind the lens where formation of an Einstein Ring gives infinite magnification for a point source, or very large magnification for a finite size source. The point-lens gives a symmetric magnification pattern $A(u)$, with u the projected source-lens distance in the source plane, in units of the Einstein Ring radius. The linear source trajectory has impact parameter u_0 and a timescale t_E , both expressed in units of the angular Einstein radius (Einstein 1936),

$$\theta_E = \sqrt{\frac{4GM}{c^2} \left(\frac{D_S - D_L}{D_S D_L} \right)}, \quad (1)$$

where M is the lens mass, and D_S and D_L are the distances

to the source and the lens respectively. This produces a symmetric lightcurve with magnification $A(u(t))$ peaking at A_0 at time t_0 . Thus 3 parameters, u_0 , t_0 , and t_E define the shape of a point-source point-lens lightcurve. Finite source effects alter the peak of the lightcurve when u_0 is of order $\rho_* = \theta_*/\theta_E$, the source star radius in Einstein radius units.

With two or more lens masses, the simple point caustic becomes a more complex set of closed curves consisting of concave segments joining at cusps, the shapes and locations depending on the lens masses and locations. Microlensing lightcurve anomalies, relative to the point-lens model, arise from the asymmetric magnification pattern associated with these caustic curves. The source trajectory may pass nearby to a cusp, causing a bump in the lightcurve, or cross over a caustic curve, resulting in a variety of complex lightcurve features, depending on the exact lens geometry. For a static binary lens, the caustic pattern depends on the mass ratio q and separation d between the two lens masses. The source trajectory relative to the caustics is specified by the impact parameter u_0 relative to the centre of mass of the lens, and the trajectory angle α relative to the line connecting the two lens masses.

As emphasised by Cassan (2008) and Kains et al. (2009), for caustic-crossing events the standard parameterisation makes it very difficult to conduct a systematic exploration of the parameter space. The alternative parameterisation formalised by Cassan (2008) replaces $(u_0, \alpha, t_0, t_E, \rho_*)$ by equivalent parameters $(s_{\text{in}}, s_{\text{out}}, t_{\text{in}}, t_{\text{out}}, \Delta t_{\text{cc}})$ that are more closely related to observable lightcurve features, and therefore better constrained by observations. Of the “standard” binary-lens microlensing parameters, two are retained: the mass ratio of the lens components q (≤ 1), and their projected separation d .

Kains et al. (2009) show that the alternative parameters are better suited to fitting caustic-crossing event lightcurves, finding models that are widely separated and easily missed with the standard binary-lens parameterisation. However, the global χ^2 minimum found in the Kains et al. (2009) analysis of OGLE-2007-BLG-472 was a model with a “planetary” mass ratio $q \sim 10^{-4}$, but with an extremely long timescale, $t_E \sim 2000$ days. This model was rejected through a qualitative discussion with the expectation that a Bayesian analysis would more naturally shift the best fit to a different local χ^2 minimum with less exotic parameters. In this paper, we add priors on relevant parameters, attempting to remove the need for such qualitative arguments by using a badness-of-fit statistic that includes both the likelihood and additional terms originating from prior information.

3 DATA

3.1 Synthetic Lightcurve Data

To test our automated algorithm, we generated a data set using the parameters given in Table 1, selected to reproduce features seen in observed anomalous microlensing lightcurves. The chosen parameters correspond to a caustic-crossing binary-lens event with crossings separated by 7 days and occurring near the lightcurve peak (Fig. 1).

For an observation at time t_i , when the source is magnified by a factor $A(t_i)$, the true model magnitude is

Parameter	Units	
t_0	5503.6	MHJD
t_E	27.2	days
α	1.68	rad
u_0	0.1	—
ρ_*	0.003	—
d	1.22	—
q	0.08	—
$g = F_B/F_S$	5	—

Table 1. Standard binary-lens parameters used to generate our synthetic data.

$$\mu_i = -2.5 \log_{10}(F_S A(t_i) + F_B), \quad (2)$$

where the un-magnified source flux F_S was chosen to be 1/5 of the blend flux F_B , which represents un-magnified stars that are blended with the microlensing target. The source-lens trajectory’s impact parameter $u_0 = 0.1$ is small enough to reach magnification $A \sim 10$ near the closest approach at time t_0 .

We obtain synthetic magnitude data m_i by using a pseudo-random number generator to sample a Gaussian distribution with mean μ_i and standard deviation σ_i , given by

$$\sigma_i = \frac{0.01}{1 + |m_0 - \mu_i|}, \quad (3)$$

where $m_0 = -2.5 \log_{10}(F_S + F_B)$ is the baseline magnitude, corresponding to the un-magnified source flux plus the blend flux. The fractional error bars are thus 1% at the baseline and decrease when the source is magnified. After generating the synthetic magnitude data, we re-scaled these error bars to obtain a χ^2 of 1 per degree of freedom for the true model. This approximates the common practice of rescaling the nominal error bars when fitting to observed microlensing lightcurves.

We employed a non-uniform cadence emulating a typical microlens observing strategy. We start with a baseline cadence of one observation per night, increasing to 3 observations per night as the event nears the peak predicted by a point-source point-lens (PSPL) fit to the earlier data. When the anomaly is detected, i.e. when the synthetic lightcurve data departs significantly from the PSPL fit, the cadence increases to 5 observations per night. From the resulting lightcurve, a random sample of N points is selected to emulate data loss, e.g. due to bad weather or technical issues.

The resulting synthetic lightcurve, retaining 199 data points, is shown on Fig. 1. A plot of the true model lightcurve with the parameters given in Table 1 is shown on Fig. 2.

3.2 OGLE-2007-BLG-472

This event was alerted during the 2007 microlensing observing season by the OGLE collaboration, and followed up from two observing sites by the PLANET collaboration. It was used as the test event by Kains et al. (2009, see that paper for full details on the data sets) to illustrate the capabilities of a modelling scheme based on the parameters defined by Cassan (2008). We use the same event here for comparison

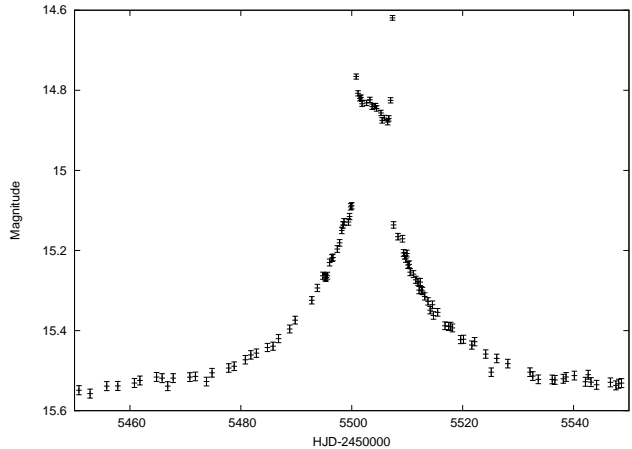


Figure 1. Synthetic data used in this paper, plotted with 1- σ error bars calculated using Eq. (3).

and in particular to show that the full Bayesian analysis shifts the posterior probability away from the exotic parameters found in the previous maximum likelihood analysis.

4 BAYESIAN FRAMEWORK

Our analysis implements a Bayesian framework for fitting microlensing events involving caustic crossings. For M parameters θ and data D , the posterior probability density in the M -dimensional parameter space is

$$P(\theta|D) = \frac{P(D|\theta) \pi(\theta)}{\int P(D|\theta) \pi(\theta) d^M \theta}. \quad (4)$$

Here $\pi(\theta)$ is the prior on the M parameters and $P(D|\theta)$ is the likelihood, e.g. for Gaussian errors with known standard deviations σ_i the likelihood is

$$L(\theta) \propto P(D|\theta) = \frac{\exp\{-\frac{1}{2}\chi^2(\theta, D)\}}{Z_D}, \quad (5)$$

with

$$\chi^2(\theta, D) = \sum_{i=1}^N \left(\frac{D_i - \mu_i(\theta)}{\sigma_i} \right)^2, \quad (6)$$

where $\mu_i(\theta)$ is the model prediction for data D_i , and

$$Z_D = (2\pi)^{N/2} \prod_{i=1}^N \sigma_i, \quad (7)$$

is a measure of the N -dimensional volume admitted by the data.

In fitting the binary lens model to microlensing lightcurve data, we project the posterior distribution in the full M -dimensional parameter space onto the (d, q) plane, a process known as *marginalising* over the $m = M - 2$ nuisance parameters, which we denote collectively by β :

$$\begin{aligned} P(d, q|D) &= \int P(d, q, \beta|D) d^m \beta \\ &= \pi(d, q) \int P(\beta|D, d, q) d^m \beta, \end{aligned} \quad (8)$$

where $\pi(d, q)$ is the prior distribution on the (d, q) plane. We take $\pi(d, q)$ to be uniform in $\log d$ and $\log q$. This choice

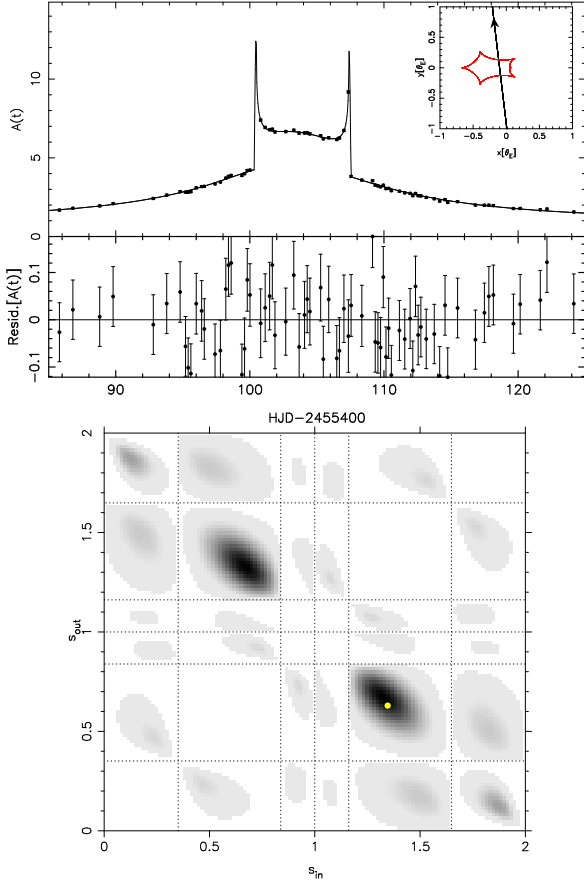


Figure 2. *Top:* Synthetic data and true model lightcurve, generated with the parameters given in Table 1. *Bottom:* The (s_{in}, s_{out}) prior map, with the location of the true model shown with a filled yellow circle.

comes from the fact that the sizes of the caustics behave like power laws of d and q .

We then marginalise over nuisance parameters by simply averaging over the samples of our Markov Chain Monte Carlo algorithm (MCMC, see e.g. Gelman et al. 1995 for more background information on this),

$$\int X(\theta) P(\beta|D, d, q) d^m \beta \approx \langle X \rangle, \quad (9)$$

where $X(\theta)$ is any function of the parameters, and we use the notation $\langle X \rangle$ to refer to a simple unweighted average over the MCMC samples. The result is a map of the posterior probability distribution $P(d, q|D)$. We will find that the maximum a posteriori (MAP) estimates of (d, q) , which maximise $P(d, q|D)$, can be quite different from the maximum likelihood (ML) estimates, which maximise $P(D|q, d, \beta)$, or minimise χ^2 .

4.1 Feature-based Parameters and Structure of the Prior $\pi(s_{in}, s_{out})$

The benefit of using the Cassan (2008) parameters $(s_{in}, s_{out}, t_{in}, t_{out}, \Delta t_{cc})$, rather than the standard parameters $(u_0, \alpha, t_E, t_0, \rho_*)$, is two-fold. First, the caustic-crossing time parameters t_{in} , t_{out} and Δt_{cc} can often be tightly con-

strained by features in the observed lightcurve. Second, the (s_{in}, s_{out}) parameters bring together onto a compact square all models that have caustic crossings at those times. In contrast, with the standard $(u_0, \alpha, t_E, t_0, \rho_*)$ parameters, the models with caustic crossings at times t_{in} and t_{out} are widely separated and difficult to locate.

The Kains et al. (2009) analysis used a genetic algorithm and assumed uniform priors on the Cassan (2008) parameters. This has obvious problems: for example, since the caustic folds that make up a caustic structure are concave (see e.g. upper panel inset of Fig. 2), a linear source trajectory cannot enter and then exit a caustic along the same caustic fold. This needs to be reflected in suitable priors on the corresponding parameters, in this example, on the (s_{in}, s_{out}) parameters, which determine where the source-lens trajectory crosses the caustic folds.

Cassan et al. (2010) derived analytic formulae for the prior $\pi(s_{in}, s_{out}|t_{in}, t_{out}, \Delta t_{cc})$, hereafter shortened to $\pi(s_{in}, s_{out})$, corresponding to a uniform isotropic distribution of source-lens trajectories, and introduced also a prior $\pi(t_E)$ on the event timescale, showing how $\pi(t_E)$ effectively modifies $\pi(s_{in}, s_{out})$. The analytic prior is proportional to the Jacobian of the transformation between the standard and Cassan (2008) parameters,

$$J = \left| \frac{\partial(u_0, \alpha, t_E, t_0, \rho_*)}{\partial(s_{in}, s_{out}, t_{in}, t_{out}, \Delta t_{cc})} \right|. \quad (10)$$

Cassan et al. (2010) evaluated this Jacobian to find the analytic form of $\pi(s_{in}, s_{out})$ corresponding to uniform priors on all standard parameters.

As can be seen in e.g. Fig. 2, the prior $\pi(s_{in}, s_{out})$ covers a compact square, since s_{in} and s_{out} run over the same range as we move around the closed caustic curve. The square naturally sub-divides into “sub-boxes”, the boundaries of which correspond to the cusps. For a caustic with N_c cusps, there are thus N_c^2 sub-boxes. However, the sub-boxes on the anti-diagonal of the (s_{in}, s_{out}) square have s_{in} and s_{out} on the same caustic fold, which cannot occur due to the concave geometry of the folds. This means that the anti-diagonal sub-boxes must have zero probability. There are thus $N_c(N_c - 1)$ sub-boxes to consider for each caustic.

The event timescale prior $\pi(t_E)$ can in principle be obtained by considering models of microlensing in the Galaxy, mapping the joint distribution of lens mass, lens and source distances, and relative proper motion onto the corresponding distribution of t_E (e.g. Dominik 2006). A convenient alternative is to use the observed distribution of t_E , e.g. from the OGLE survey. Caution is needed because of possible biases in fitting t_E to observed lightcurves, and selection effects lowering the occurrence of short and long t_E events in the survey. Cassan et al. (2010) considered two different priors on t_E to illustrate their effect on $\pi(s_{in}, s_{out})$. One was a distribution of event timescales observed in past microlensing seasons, and another was the model distribution of Wood & Mao (2005). These two distributions were shown to be in excellent agreement with each other.

In this paper we derive a 2-dimensional joint prior on the event timescale and source size using simulations of synthetic stellar population obtained with the Besançon model (Robin et al. 2003). We briefly describe our method to derive this in the next section.

4.1.1 Deriving priors from a Galactic model

The initial maximum likelihood analysis of the microlensing event OGLE-2007-BLG-472 (Kains et al. 2009) suggests an unusual parameter combination as best description of the data. The strength and plausibility of such an approach can be tested by using a Galactic model that reflects our prior knowledge of the Galactic structure. For interpreting microlensing lightcurves, different Galactic models (Han & Gould 1995, Bennett & Rhie 2002, Dominik 2006) are in use. These models differ in details of the assumed spatial, kinematic, and mass distributions of the Galactic Bulge and Disk stellar populations. A different model which is adapted to reflect the observed star counts in the optical and near-infrared is the so-called Besançon model (Robin et al. 2003). As indicated by Kerins et al. (2009), this model can be used to predict the optical depth of gravitational microlensing events. Moreover it can be used to set detailed parameter constraints when combined with the adapted parameter estimates and the source star properties.

Based on the available online catalogue simulation, we generated a sample of stars between Earth and 11 kpc. To ensure that potential lenses, which are typically faint, are included, the apparent magnitude was not constrained. Based on the value used in the previous paper (Kains et al. 2009), we assumed a visual extinction $A_V = 0.7 \text{ mag kpc}^{-1}$, where the resulting model extinction curve stops increasing after several kpc. For a more accurate description, the calibrated spatial extinction in K_S (Marshall et al. 2006) could have been used, but this would have required a calibration for the I band, which is typically used in microlensing observations.

In order to infer microlensing distributions from the simulation, lens-source pairs were randomly drawn from the sample. These were then accepted or rejected depending on the area of their corresponding angular Einstein ring, which gives the instantaneous lensing probability. The simulated bolometric magnitude and effective temperature allowed us to estimate ρ_* . Including the simulated proper motion provided us with an estimate for the Einstein time - the only observable parameter directly connected to the lens mass. We did not include the lens-source relative proper motion in the resampling procedure, but this would lead to a distribution that favours shorter Einstein times, as fast lenses lead to larger detection zones on the sky. This is a consequence of moving the lensing cross-section of the instantaneous lensing probability along the lens-source relative proper motion. The correction depends on the annual survey observation and the survey efficiency in tE. For events much longer than the sampling rate, the increase in lensing probability can be modelled as a stripe on the sky. For a coverage of 240 days which we assume here, the actual prior distribution of the event duration changes its expected value by an amount that is negligible in comparison to the error ellipse of instantaneous case.

Our estimates illustrate that the value found by Kains et al. (2009) for t_E is much larger and that of ρ_* much smaller than typical samples drawn from the Besançon model. Consequently, we determine a bivariate Gaussian prior based on the covariance matrix of t_E and angular

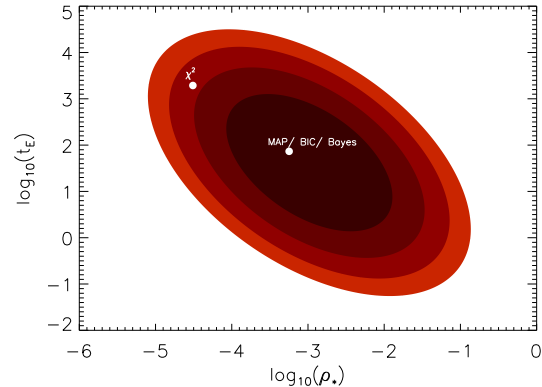


Figure 3. Contour plot of the the logarithm of our joint prior on ρ_* and t_E . The location of the best-fit models identified for event OGLE-2007-BLG-472 are shown with white filled circles and labelled for the different statistics we use, as discussed in the text.

source star radius of the simulated sample. This joint prior is plotted on Fig. 3.

Since trajectories requiring very large values of t_E and/or very small ρ_* are suppressed by this prior, so too are the corresponding regions of the $(s_{\text{in}}, s_{\text{out}})$ plane. That is, for given values of t_{in} and t_{out} , regions of $(s_{\text{in}}, s_{\text{out}})$ where the source enters and exits the caustic structure very close to the same cusp are suppressed. This is evident on the $\pi(s_{\text{in}}, s_{\text{out}})$ maps, e.g. the bottom panel of Fig. 2, where the prior is low in the corners along the anti-diagonal line.

Because the Cassan (2008) parameters assume that the source trajectory crosses a caustic, and because we are comparing caustics of different sizes as we move across the (d, q) plane, a full implementation of the uniform isotropic prior on source-lens trajectories must account for large caustics being easier to hit than small ones. If two models have equal χ^2 but cross caustics of different sizes, the prior should favour the model with a larger probability of being hit. As each $(s_{\text{in}}, s_{\text{out}})$ corresponds to a different source trajectory angle α , we quantify this by defining $\pi_H(d, q, \alpha)$, the probability that a caustic will be “hit” by a trajectory with angle α . This is proportional to the range of impact parameters intersecting the caustic, i.e. the projected size of the caustic perpendicular to the source trajectory. The concave structure of the caustic means that once the N_c cusp positions are found, and rotated by an angle $-\alpha$, the vertical range then gives the projected cross-section of the caustic. Thus if the Cassan et al. (2010) prior $\pi(s_{\text{in}}, s_{\text{out}})$ is normalised to 1 when integrated over the $(s_{\text{in}}, s_{\text{out}})$ square, the full prior multiplies this by $\pi_H(d, q, \alpha)$.

4.2 Automated modelling scheme

The flowchart in Fig. 4 summarises the main steps of our automated modelling scheme. In summary,

- (i) For each node in the (d, q) grid, we construct the corresponding caustic curves.
- (ii) For each caustic curve, we construct the $\pi(s_{\text{in}}, s_{\text{out}})$ prior map, which divides into sub-boxes.
- (iii) In each sub-box, we launch an MCMC run on the β

parameters to find the best fit and map out the posterior $P(\beta|D, d, q, \text{box})$. Chains are kept confined to each sub-box by forcing MCMC steps to remain within its boundaries.

The results are then collected to construct the posterior probability $P(d, q|D)$, either by optimising the nuisance parameters or by integrating over the nuisance parameters in each sub-box, and then summing over the sub-boxes. Finally, we compute the corresponding ‘‘Badness-of-Fit’’ statistic $\text{BoF}(d, q) = -2 \ln P(d, q|D)$.

Our automated modelling scheme exploits the structure of the prior $\pi(s_{\text{in}}, s_{\text{out}})$. For a caustic with N_c cusps, the prior $\pi(s_{\text{in}}, s_{\text{out}})$ has $N_c(N_c - 1)$ local maxima, one in each of the sub-boxes. As the separation between these local maxima can be large, a single MCMC run, or whichever other parameter optimisation method is employed, may find it difficult to jump from one sub-box to another, and thus may fail to find the best solution. To avoid this, we launch an MCMC run in *each* of the sub-boxes. Thus we start $N_c(N_c - 1)$ chains, each confined to a particular sub-box, to locate the best fit in each sub-box. We stop the chains using the convergence criterion of Geweke (1992) once they are past a minimum number of iterations.

Our method thus divides the binary-lens parameter space not only into a (d, q) grid, but further into the required sub-boxes for each caustic for each (d, q) pair. In each sub-box we start the MCMC run at the maximum of $\pi(s_{\text{in}}, s_{\text{out}})$. Instead of using χ^2 as the sole criterion for acceptance or rejection of proposed MCMC steps, the ratio of the priors is also taken into account.

To incorporate non-uniform priors $\pi(\theta)$ in the MCMC algorithm, we simply modify the criterion for accepting a proposed step. Rather than only the likelihood $P(D|\theta)$, we consider the full posterior $P(\theta|D) \propto P(D|\theta)\pi(\theta)$. A proposal to take a random step from θ to θ' is always accepted if θ' increases the posterior, and the acceptance probability when θ' diminishes the posterior is the ratio of posterior probabilities

$$\frac{P(\theta'|D)}{P(\theta|D)} = \exp\left(-\frac{1}{2}\Delta\chi^2\right) \frac{\pi(\theta')}{\pi(\theta)}, \quad (11)$$

where $\Delta\chi^2 = \chi^2(\theta') - \chi^2(\theta)$ is the difference in χ^2 across the proposed step. For an MCMC run over the full parameter set θ , the relevant prior is

$$\pi(\theta) = \pi(d, q) \pi(\beta|d, q). \quad (12)$$

For MCMC runs over the nuisance parameters β , with fixed d, q , the relevant prior is

$$\pi(\beta|d, q) \propto \pi(s_{\text{in}}, s_{\text{out}}) \pi_{\text{H}}(d, q, \alpha). \quad (13)$$

4.3 Implementation

We implemented the algorithm by using a cluster of desktop computers, each one running one of the MCMC chains to map out the posterior $P(\beta|D, d, q, \text{box})$ for a grid of (d, q) values and for all the corresponding sub-boxes. The results are then collected to construct the posterior probability map $P(d, q|D)$, integrating over the nuisance parameters β , and summing over the sub-boxes.

$P(d, q|D, \text{box})$ is evaluated from each MCMC chain using the best-fit parameters $\hat{\beta}$:

$$P(d, q|D, \text{box}) \propto P(D|d, q, \text{box}, \hat{\beta}) \pi(\hat{\beta}|d, q, \text{box}). \quad (14)$$

Because each sub-box has its own MCMC chain, we must weight the chain averages by the prior probability of each sub-box:

$$\pi(\text{box}|d, q) = \iint \pi(s_{\text{in}}, s_{\text{out}}) \pi_{\text{H}} ds_{\text{in}} ds_{\text{out}}, \quad (15)$$

where the integration limits cover the sub-box. The weighted sum of chain averages then gives the posterior (d, q) map,

$$P(d, q|D) = \sum_{\text{box}} \pi(\text{box}|d, q) P(d, q|D, \text{box}). \quad (16)$$

Normally one sub-box dominates the sum, but sometimes two or more can contribute.

5 RESULTS

5.1 Badness-of-Fit Criteria

We consider and compare results for four alternative ‘‘Badness-of-Fit’’ criteria, corresponding to maximum likelihood (ML), maximum a-posteriori (MAP), and the Bayesian Information Criterion (BIC), as well as a Bayes statistic that integrates the posterior probability over the nuisance parameters. In each case the best-fit parameters (d, q) minimise a ‘‘Badness-of-Fit’’ statistic, $\text{BoF}(d, q)$, and the corresponding posterior probability is $P(d, q|D) \propto \exp\{-\frac{1}{2}\text{BoF}(d, q)\}$. Figs 6-8 display the $\text{BoF}(d, q)$ maps obtained for the four cases:

$$\begin{aligned} \text{ML} : & \quad \text{BoF} = \chi^2(\hat{\beta}) \\ \text{MAP} : & \quad \text{BoF} = \chi^2(\hat{\beta}) - 2 \ln \pi(\hat{\beta}) \\ \text{BIC} : & \quad \text{BoF} = \chi^2(\hat{\beta}) - 2 \ln \pi(\hat{\beta}) + \ln(N_D) N_{\text{eff}} \\ \text{Bayes} : & \quad \text{BoF} = \chi^2 - 2 \ln(\pi(\beta) d^m \beta). \end{aligned}$$

Here the prior π is from Eqn. 12 or Eqn. 13, depending on the context. We briefly elaborate on the three options below before discussing the results.

- **ML:** The *maximum likelihood* (ML) parameters maximise the likelihood $L(d, q) = P(D|d, q)$, equivalent to minimising $\text{BoF} = -2 \ln(L) = \chi^2$. Thus we determine the best-fit value of χ^2 for each (d, q) pair, and let $P(d, q|D) \propto \exp(-\chi^2/2)$. This approach emphasises the fit to the data while disregarding priors on the parameters.

- **MAP:** The *maximum a-posteriori* (MAP) parameters maximise the posterior probability density $P(d, q|D)$, equivalent to minimising $\text{BoF}(d, q) = -2 \ln P(d, q|D)$.

- **BIC:** The *Bayesian Information Criterion* (BIC), applies an ‘‘Occam’’ penalty that gives priority to ‘‘simpler’’ models that employ fewer parameters to achieve their fit. Each (d, q) grid point is regarded as a competing model with equal prior probability and N_{eff} effective parameters that have been optimised. The *Akaike Information Criterion* (AIC) uses an Occam penalty $2 N_{\text{eff}}$ (Akaike 1974), while the *Bayesian Information Criterion* (BIC) uses a stronger penalty $\ln(N_D) N_{\text{eff}}$, with N_D the number of data points (Schwarz 1978). Our tests with fitting of polynomial models

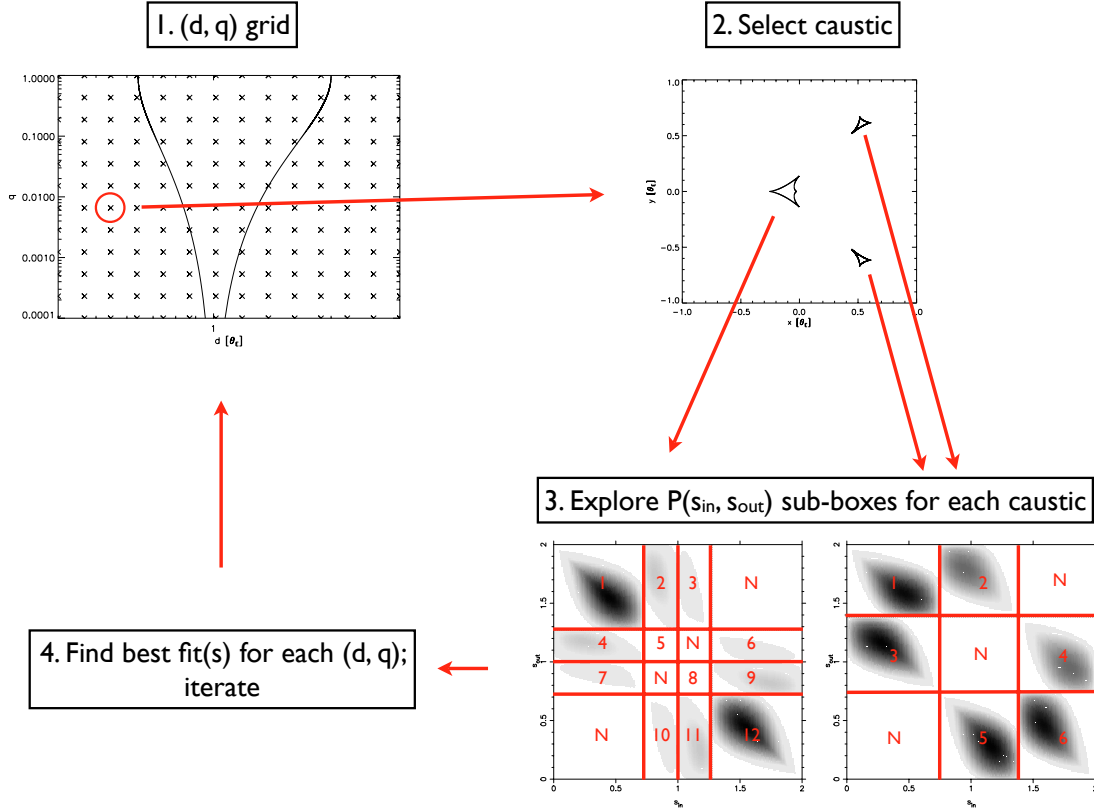


Figure 4. Algorithm flow for our modelling scheme. In the bottom right panel, “N” denotes an empty sub-box, while the other non-empty sub-boxes are enumerated.

suggest that the BIC may be more reliable than the AIC for model selection.

We use the MCMC samples to estimate the “effective number” of nuisance parameters,

$$N_{\text{eff}} \approx \langle D(\theta) \rangle - D(\langle \theta \rangle), \quad (17)$$

where $\langle x \rangle$ denotes the expectation value of x under the posterior, simply calculated by taking an unweighted average over the MCMC samples, and the ‘deviance’ is

$$D(\theta) \equiv \chi^2 - 2 \ln \pi, \quad (18)$$

as used to compute the acceptance probability of each step in the MCMC algorithm, as per Eq. (11). Here $D(\langle \theta \rangle)$ estimates the deviance at the minimum, while $\langle D(\theta) \rangle$ measures the typical value, which should rise by 1 for each dimension of the parameter space explored by the MCMC samples. This definition of N_{eff} is designed to avoid double-counting when two parameters are highly correlated, and is found in the *Deviance Information Criterion* (DIC, Spiegelhalter et al. 2002, see also Ando 2007).

• **Bayes:** A fully Bayesian approach integrates the posterior probability density over the m nuisance parameters β , rather than just finding the maximum likelihood (ML) or maximum posterior probability density (MAP). Thus if two models have the same MAP statistic, the one that achieves that good fit over a wider range of parameters has a correspondingly higher probability.

We can also write out the Bayes statistics as

$$\text{BoF} = \chi^2(\hat{\beta}) - 2 \ln \pi(\hat{\beta}) - \sum_{i=1}^m \ln (2\pi \lambda_i(\hat{\beta})), \quad (19)$$

where the 2π factor here refers to the constant $\pi = 3.141592\dots$ rather than the prior $\pi(\beta)$, and $\lambda_i(\hat{\beta})$ are the m eigenvalues of the parameter-parameter covariance matrix evaluated at $\hat{\beta}$, their product being the m -dimensional parameter volume admitted by the data around the best-fit value $\hat{\beta}$.

We approximate the integral over the m nuisance parameters by the method of steepest descents,

$$\int e^{-\chi^2(\beta)/2} \pi(\beta) d^m \beta \approx e^{-\chi^2(\hat{\beta})/2} \pi(\hat{\beta}) d^m \beta \quad (20)$$

$$\approx e^{-\chi^2(\hat{\beta})/2} \pi(\hat{\beta}) \prod_{i=1}^m (2\pi \lambda_i(\hat{\beta}))^{1/2}, \quad (21)$$

where the 2π factor here again refers to the constant rather than the prior. This is just the MAP statistic multiplied by a parameter space volume. We evaluate parameter space volume $d^m \beta$ as the square root of the determinant of the parameter-parameter covariance matrix derived from the MCMC chain.

5.2 Fits to synthetic data

For the synthetic event there is a single narrow, well-defined minimum. Table 2 summarises the parameters of the best-

Parameter		Units
d (grid)	1.237	–
q (grid)	0.059	–
$g = F_B/F_S$	5.81 ± 0.09	–
χ^2	202.9	–
“Standard”		
t_0	5503.62 ± 0.014	MHJD
t_E	37.52 ± 0.04	days
α	1.692 ± 0.005	rad
u_0	0.056 ± 0.003	–
ρ_*	$(2.44 \pm 0.26) \times 10^{-3}$	–
“Caustic”		
t_{in}	5500.394 ± 0.009	MHJD
t_{out}	5507.342 ± 0.004	MHJD
s_{in}	1.273 ± 0.002	–
s_{out}	0.706 ± 0.002	–
Δt_{cc}	0.092 ± 0.010	days

Table 2. Best-fit parameters (from d, q grid exploration) for the synthetic event.

fit model found with a 14×14 (d, q) grid, evenly spaced in $\log d$ and $\log q$. The posterior distribution $P(d, q|D)$ found using the MAP option is plotted in Fig. 5; the ML and BIC posterior maps are almost undistinguishable. The BoF minimum is so tightly defined that the choice of BoF statistic has little effect on the best-fit parameters or the shape of the posterior map.

The fit that is recovered is located at the grid point closest to the true model, as can be seen by comparing Fig. 5 to Fig. 2, and the best-fit parameters given in Table 2 to Table 1. The true parameters are not exactly recovered, as they do not match our grid points, but another modelling could be conducted without keeping d and q fixed, using the best models for each grid point as a starting point for new MCMC runs.

5.3 Fits to OGLE-2007-BLG-472 data

Our fits to the OGLE-2007-BLG-472 data are presented in Figs 6-8. The contour levels are set at $\Delta\text{BoF}=2.3, 6.17, 11.8, 20, 50, 100, 250$ and 500 , relative to the global minimum, the first 3 thus corresponding to 1, 2, and 3- σ confidence regions if the posterior is well approximated by a 2-parameter Gaussian. The best-fit values and uncertainties of additional parameters are summarised in Table 3.

Fig. 6 exhibits an extended region of low χ^2 around the minimum at $d = 0.51$ and $q = 2 \times 10^{-4}$. The width in d is unresolved by the rather coarse (d, q) grid, and the extension in $\log q$ is around 1 dex. The best-fit model has the source crossing a very small planetary caustic, requiring a very long event timescale, $t_E \sim 2000$ d, to match the observed crossings at t_{in} and t_{out} separated by 3 d. Thus, as was also found in Kains et al. (2009), the lowest- χ^2 model for this event is not very well constrained, and has an implausibly long t_E . There are no significantly different competing local minima with $\Delta\chi^2 < 20$; the first competitive model for which the configuration (source trajectory and location of the caustic crossings) is significantly different has $\Delta\chi^2 \sim 22$.

Changing the BoF statistic has a significant effect on the posterior map: the penalties introduced by the prior move the best-fit model “up” in q , towards models with smaller t_E and configurations where the source crosses a central, rather than planetary, caustic. The MAP, BIC and Bayes fits (Fig. 7 - 8) all favour a model with $q \sim 0.12$, $d \sim 0.61$.

The χ^2 increases by $\Delta\chi^2 = 43$ relative to the global χ^2 minimum, but the priors compensate since t_E and ρ_* both move toward more plausible values, and the larger caustic is easier to hit. Fig. 3 shows the location of the lowest- χ^2 and best Bayesian models with respect to the $\pi(\rho_*, t_E)$ contour. The χ^2 model is in the wings of the prior distribution, whereas the best-BIC model is near its peak, meaning that the χ^2 model is more strongly penalised by the prior.

We used the best-fit Bayesian parameters (Table 3) and the algorithm of Dominik (2006) to derive probability distributions for the lens mass and distance as shown in Fig. 9. With no parallax signal detected in this event, we used only the constraint from t_E and ρ_* . We find lens component masses of $0.78^{+3.43}_{-0.47} M_\odot$ and $0.11^{+0.47}_{-0.06} M_\odot$ at a distance of $5.88^{+1.49}_{-2.68}$ kpc.

The best Bayesian model has a large blend/source flux ratio $F_B/F_S \sim 200$. There is no obvious star blended with the lens on the images, and the blending could plausibly come from the binary-star lens system, or from a third body.

6 DISCUSSION AND CONCLUSIONS

The modelling results for the two datasets presented here indicate that our algorithm is successful in locating minima throughout the parameter space, and the subdivision of the prior maps ensures that all possible source trajectories through the caustics are explored. Furthermore, the use of Bayesian priors allows us to incorporate information on the event timescale distribution, as well geometrical information on the concavity of caustics.

Although the sampling rate for our synthetic lightcurve data is not particularly high compared to what can now be achieved by survey and follow-up teams, our algorithm located a well-defined minimum near the true minimum, with a grid search of the (d, q) parameter space and MCMC runs to sample the posterior probability in the region around each local minimum.

In our re-analysis of the OGLE-2007-BLG-472 data, we improve upon the posterior map calculated in Kains et al. (2009) for OGLE-2007-BLG-472 because we now use an MCMC run for each prior sub-box separately rather than just a single one per (d, q) grid point. We find that changing the badness-of-fit statistic leads to important changes in the posterior $P(d, q|D)$ maps. In particular, the model with lowest χ^2 has a planetary mass ratio and an implausibly long $t_E \sim 2000$ d. Adding priors dramatically shifts the location of the best-fit model, lowering the timescale to $t_E \sim 70$ d. Using a Bayesian approach to penalise models with improbable parameters leads to best-fit parameters corresponding to a binary star lens with 0.78 and 0.12 M_\odot components at a distance of ~ 5.9 kpc, and a more typical event timescale $t_E \sim 70$ d. The only remarkable parameter is a rather high blending fraction, which could arise from either the lens itself or a closely blended third star. The new model is very different from that found by Kains et al. (2009), which char-

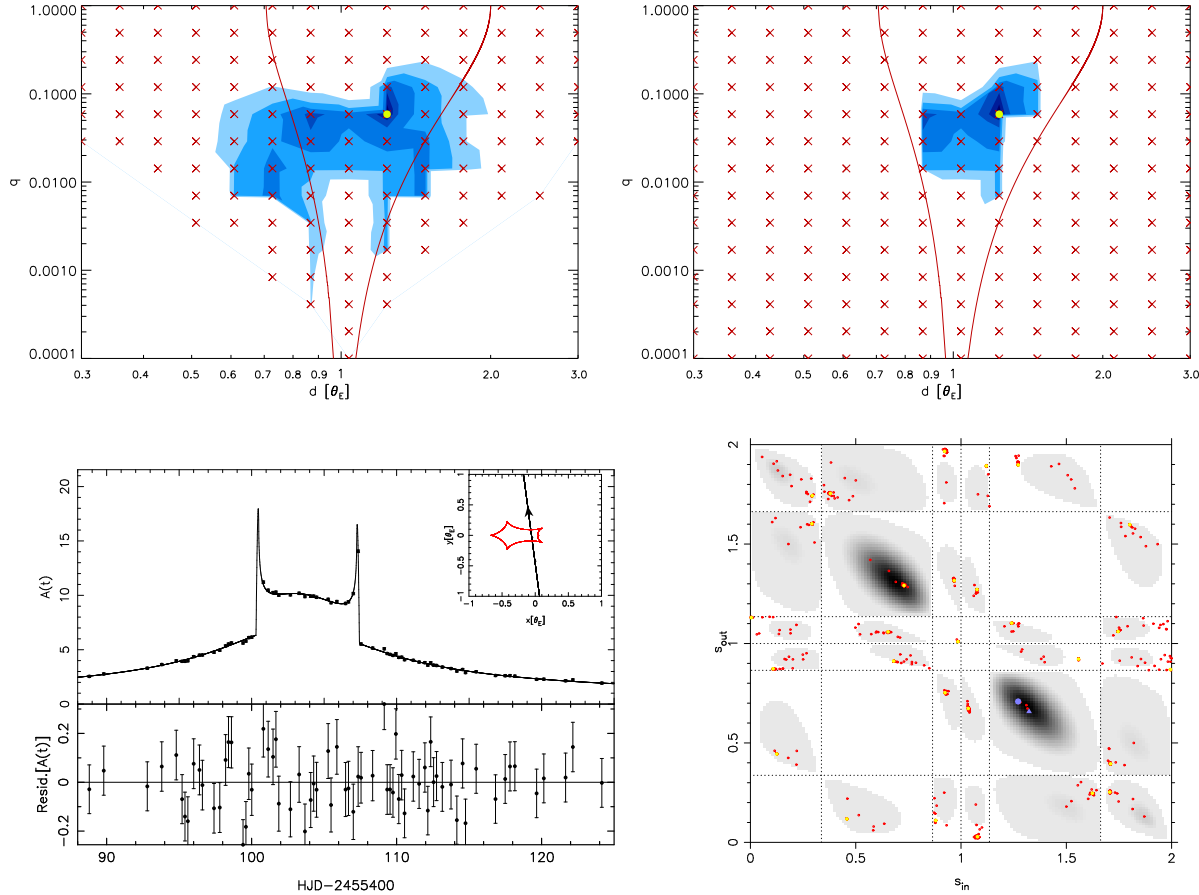


Figure 5. MAP fit to the synthetic lightcurve data, using BoF = $\chi^2(\hat{\beta}) - 2 \ln \pi(\hat{\beta})$. *Top:* Posterior maps $P(d, q|D)$ for the source crossing a central (left) and secondary (right) caustic. Contour levels are at $\Delta\text{BoF} = 2.3, 6.17, 11.8, 20, 50, 100, 250$. The model with the lowest BoF is marked with a yellow filled circle and that of the true model with a filled blue triangle. *Bottom:* The data and best-fit model lightcurve, with an inset showing the source trajectory crossing the caustic (left), and the location (yellow filled circle) of the best-fit model on the prior map $P(s_{in}, s_{out})$, along with MCMC samples (red circles) and local best-fit minima in each sub-box, indicated by yellow circles (right).

acterised the lens as a binary star with components masses of 1.50 and $0.12M_{\odot}$ at a distance of 1 kpc.

The development of automated algorithms for real-time modelling such as that presented here allows observers to receive feedback on ongoing anomalous microlensing events, and ensure that important features predicted by real-time modelling are not missed. This makes it much easier to assess the nature of the lensing system more rapidly and allocate observing time to targets more effectively. When observational coverage is not complete, or when the χ^2 alone is not sufficient as a criterion for badness-of-fit, statistics like the those we use in this paper could help to assess reliably alternative models. Furthermore, provided that the chosen priors are appropriate, comparing the resulting posterior maps of using different statistics allows for a useful test of a given model’s robustness.

ACKNOWLEDGMENTS

NK is supported by an ESO Fellowship. The research leading to these results has received funding from the European Community’s Seventh Framework Programme (/FP7/2007-

2013/) under grant agreement No 229517. KH and MH are supported by The Qatar Foundation QNRF grant NPRP-09-476-1-87.

References

- Akaike H., 1974, IEEE Transactions on Automatic Control, 19, 716
- Ando T., 2007, Biometrika, 94, 443
- Beaulieu J.-P., et al., 2006, Nature, 439, 437
- Bennett D. P., Rhie S. H., 2002, ApJ, 574, 985
- Cassan A., 2008, A&A, 491, 587
- Cassan A., Horne K., Kains N., Tsapras Y., Browne P., 2010, A&A, 515, A52+
- Cassan A., Kubas D., Beaulieu J.-P., et al., 2012, Nature, 481, 167
- Dominik M., 2006, MNRAS, 367, 669
- Einstein A., 1936, Science, 84, 506
- Gelman A., Carlin J., Stern H., Rubin D., 1995, Bayesian Data Analysis, Chapman & Hall, London

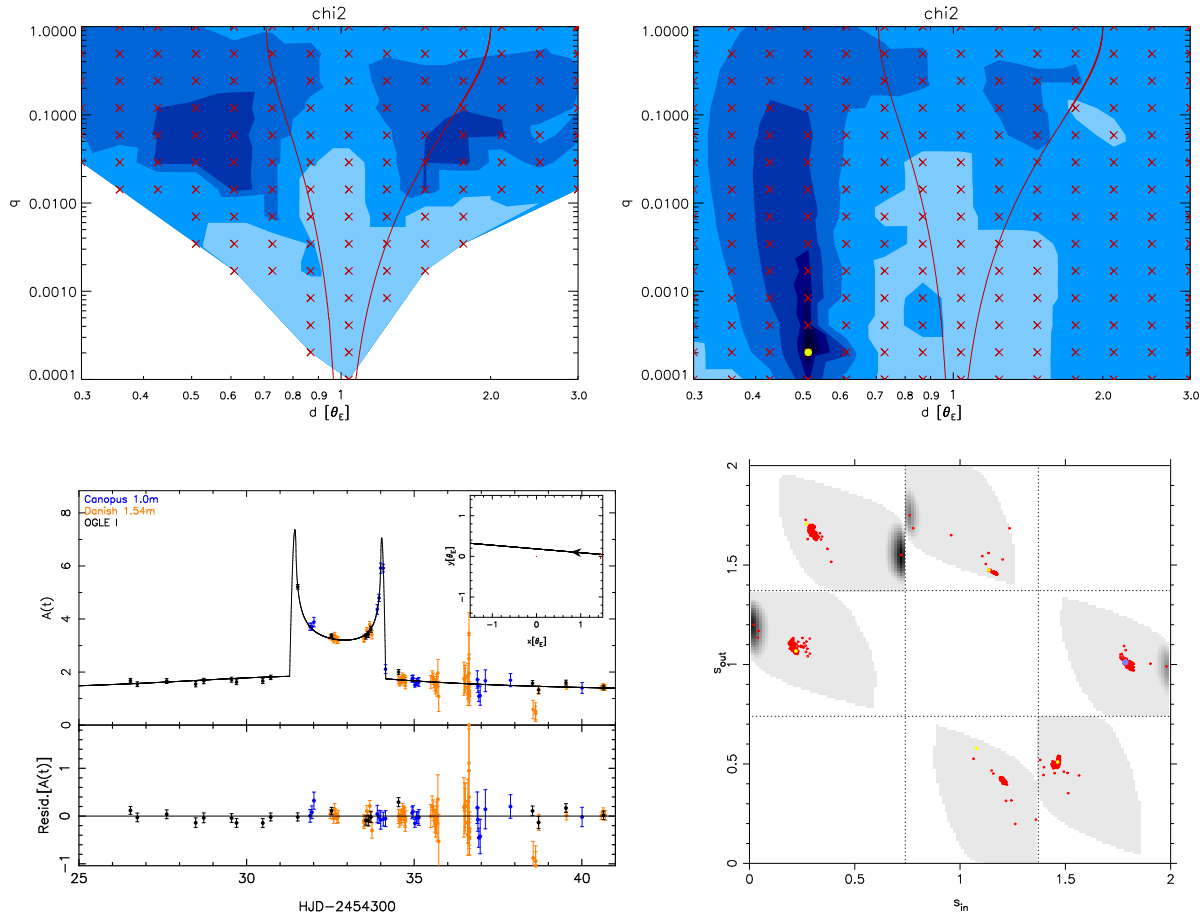


Figure 6. ML fit to the OGLE-2007-BLG-472 data, using $\text{BoF} = \chi^2$. *Top:* Posterior maps $P(d, q|D)$ for the source crossing the central caustic (*left*) and the secondary caustic (*right*). A filled yellow circle marks the location of the model with the lowest χ^2 , and the contour levels are at $\Delta\chi^2 = 2.3, 6.17, 11.8, 20, 50, 100, 250$. *Bottom:* The data and best-fit model lightcurve (*left*), with an inset showing the source trajectory and the caustic, and the prior map $P(s_{in}, s_{out})$ (*right*), along with the MCMC samples (red circles) and local best-fit minima (yellow circles) in each sub-box. The best-fit model is marked by a blue filled circle.

Geweke J., 1992, Bayesian Statistics 4, Oxford University Press, J. M. Bernardo, J. O. Berger, A. P. Dawid and A. F. M. Smith (eds)

Han C., Gould A., 1995, ApJ, 449, 521

Kains N., Cassan A., Horne K., et al., 2009, MNRAS, 395, 787

Kerins E., Robin A. C., Marshall D. J., 2009, MNRAS, 396, 1202

Kubas D., et al., 2005, A&A, 435, 941

Mao S., Paczyński B., 1991, ApJ, 374, L37

Marshall D. J., Robin A. C., Reylé C., Schultheis M., Picaud S., 2006, A&A, 453, 635

Muraki Y., Han C., Bennett D. P., et al., 2011, ApJ, 741, 22

Paczynski B., 1986, ApJ, 304, 1

Robin A. C., Reylé C., Derrière S., Picaud S., 2003, A&A, 409, 523

Schwarz G., 1978, Ann. Statist., 21, 461

Spiegelhalter D., Best N., Carlin B., van der Linde A., 2002, J.R. Statist. Soc. B, 64, 583

Wood A., Mao S., 2005, MNRAS, 362, 945

This paper has been typeset from a $\text{T}_{\text{E}}\text{X}/\text{L}^{\text{A}}\text{T}_{\text{E}}\text{X}$ file prepared by the author.

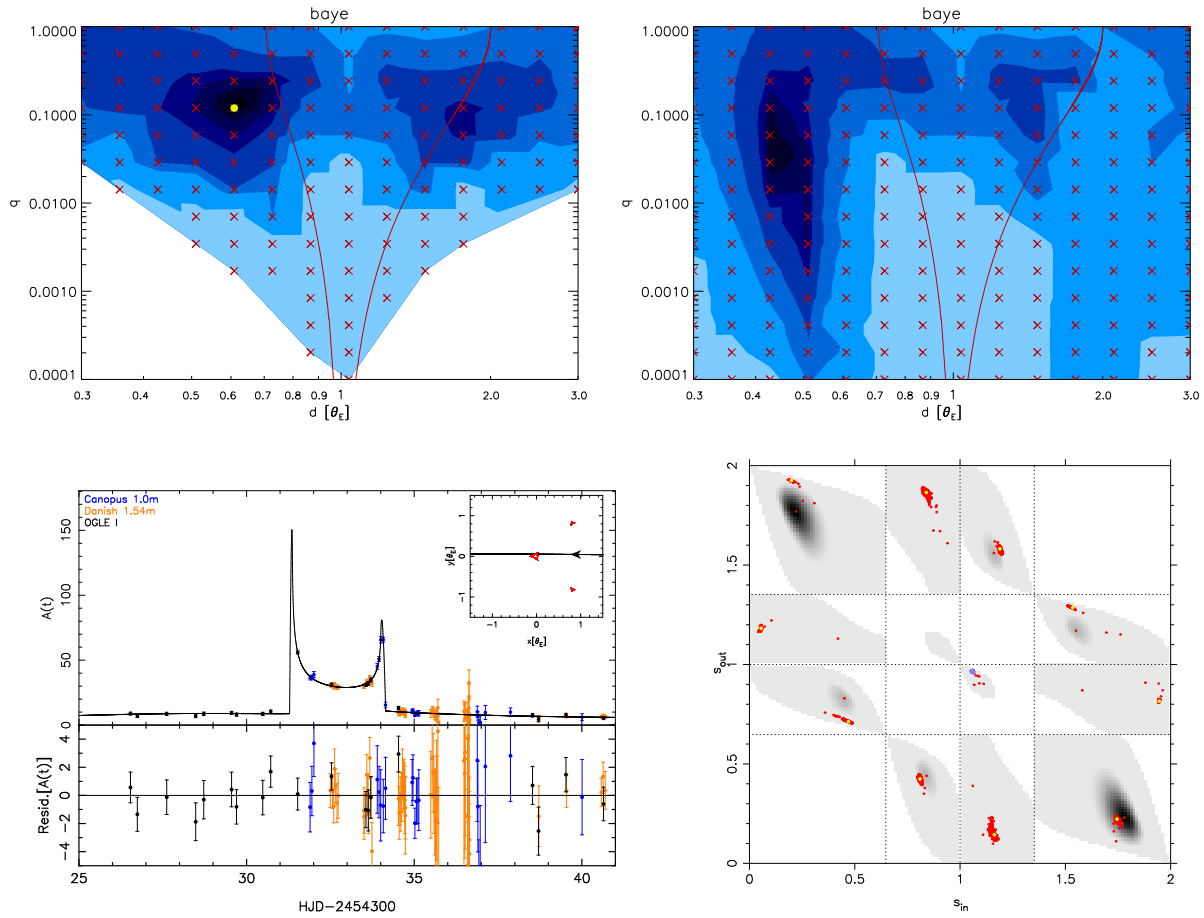


Figure 7. Same as Fig. 6 but for a fully Bayesian fit using $\text{BoF} = \chi^2 - 2 \ln(\pi(\beta) d^m \beta)$, thus augmenting the likelihood with suitable Bayesian priors on the parameters and taking into account the effective number of parameters, as detailed in the text. Corresponding figures for a MAP and BIC fit are shown on Fig. 8 for comparison.

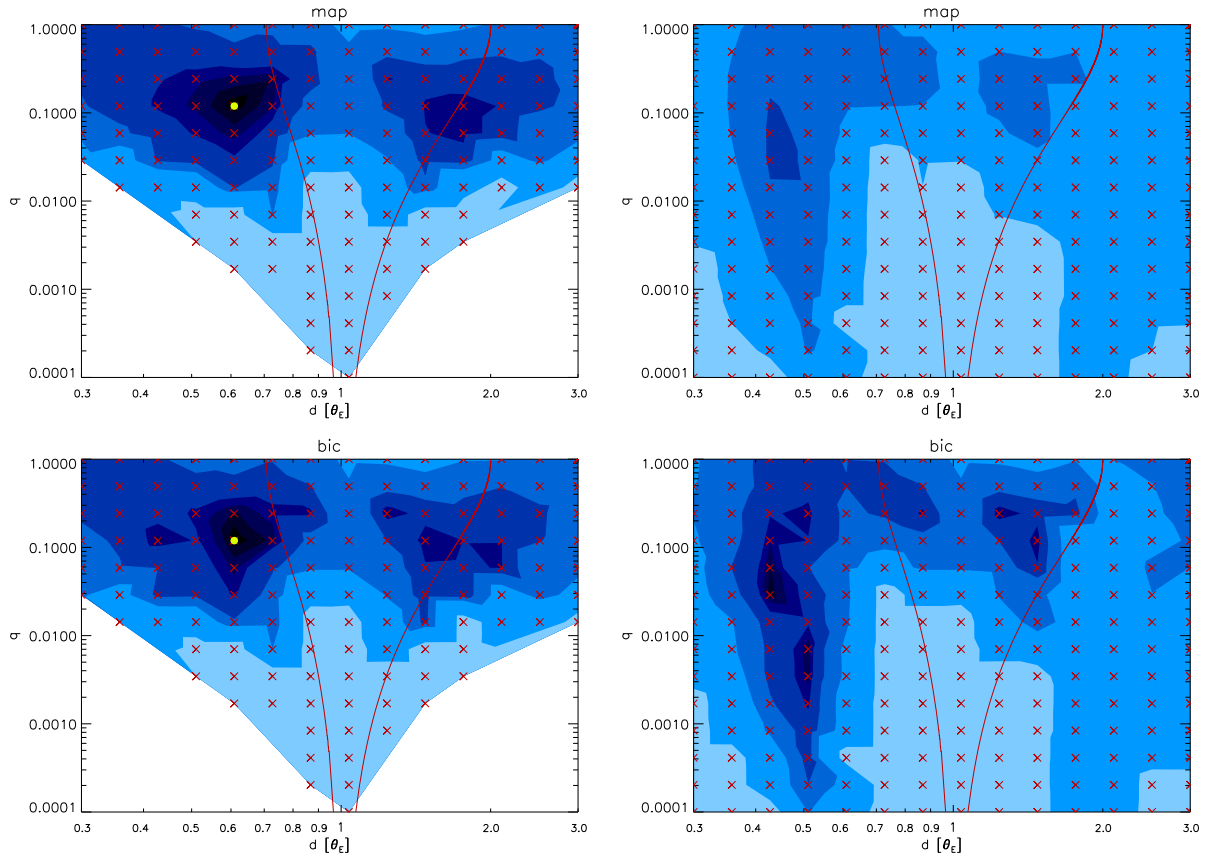


Figure 8. Posterior maps using the MAP and BIC statistics for comparison with the “Bayes” map (Fig. 7); maps for central caustic crossings are shown at the left, with secondary caustic crossings shown on the right.

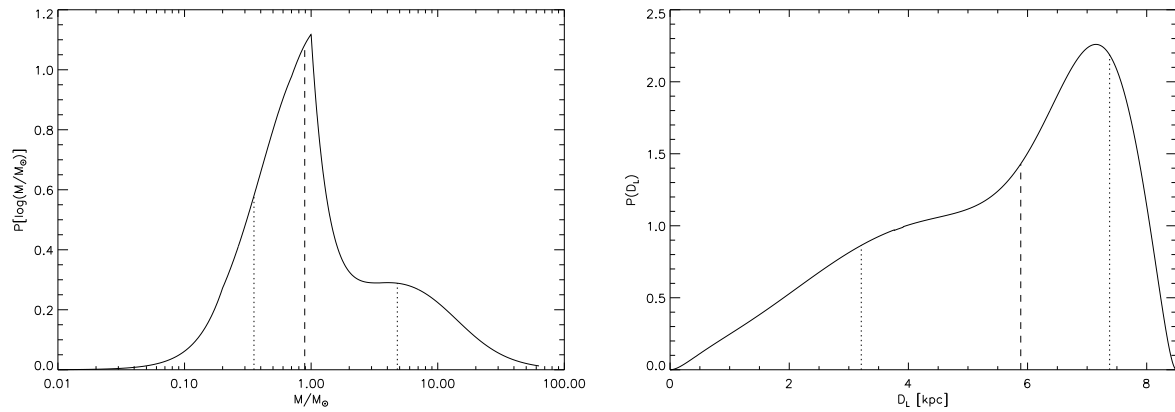


Figure 9. Probability density distributions for the lens mass (left) and distance (right) using the best-fit parameters found by minimising the BIC, computed using the algorithm of Dominik (2006). The distance distribution assumes a source distance $D_S = 8.5$ kpc. Dashed lines and dotted lines respectively denote the median value and the limits of the 68.3% confidence interval.

Parameter	ML (Fig. 6)	MAP/BIC/Bayes (Fig. 7)	Units
ML (χ^2)	915	958	–
MAP	1017	968	–
BIC	1046	986	–
Bayes	1061	1003	–
d (grid)	0.51	0.61	–
q (grid)	2.03×10^{-4}	0.119	–
$g = F_B/F_S$ (OGLE)	7.59 ± 0.08	114.59 ± 9.62	–
N_{eff}	4.20	4.97	–
Standard			
t_0	7121.28 ± 113.61	4332.41 ± 0.25	MHJD
t_E	1939.35 ± 80.92	73.37 ± 5.45	day
α	3.134 ± 0.044	3.050 ± 0.020	rad
u_0	-0.181 ± 0.029	-0.052 ± 0.003	–
ρ_*	$(3.09 \pm 0.37) \times 10^{-5}$	$(5.66 \pm 0.51) \times 10^{-4}$	–
“Caustic”			
t_{in}	31.379 ± 0.012	31.325 ± 0.016	MHJD-4300
t_{out}	34.078 ± 0.002	34.077 ± 0.002	MHJD-4300
s_{in}	1.785 ± 0.012	0.807 ± 0.005	–
s_{out}	1.011 ± 0.013	0.423 ± 0.011	–
Δt_{cc}	0.073 ± 0.003	0.072 ± 0.004	day
I_s	17.95	20.77	mag
I_b	15.74	15.62	mag
θ_*	1.15	0.53	μas

Table 3. Best-fit standard (top) and “caustic” (middle) parameters for OGLE-2007-BLG-472, as well as source properties and blend magnitude (bottom), for the ML and BIC statistics. The values of all 4 BoF statistics are given for both models for informative purposes. d and q are fixed since these are grid models. Source angular radii are computed using the same colour as in the previous paper on this event (Kains et al. 2009).